Tellus (1989), *41A*, 401–415

A laboratory model of severe downslope winds

By JAMES W. ROTTMAN*, *Department of Marine, Earth and Atmospheric Sciences, North Carolina State University, Raleigh, NC 27695, USA* and RONALD B. SMITH, *Department of Geology and Geophysics, Yale University, New Haven, CT 06511, USA*

(Manuscript received 6 April 1988; in final form 23 January 1989)

ABSTRACT

Laboratory experiments are described in which flow visualization techniques were used to investigate the conditions under which a severe downslope wind may exist for linearly stratified flow over a ridge when the upstream flow is shear free. Three different ridges with similar cross sections but with maximum slopes of 40°, 27° and 13° were used. In the experiments for each ridge, the Froude number $F = U/(NH)$, where U is the free stream speed, N is the buoyancy frequency and H is the ridge height, was varied over the full range in which internal wave breaking was anticipated. The range of F over which a well-mixed region of turbulent fluid formed above the ridge was determined for each of the three ridges. This well-mixed region was observed to occur generally in conjunction with a strong downslope flow on the lee side of the ridge. The results of the laboratory experiments are compared with previous numerical simulations and with a nonlinear hydrostatic theory for severe downslope winds.

1. Introduction

Incidents of severe winds on the lee sides of mountains have been reported for many of the world's major mountain ranges. The Boulder windstorm on the eastern slopes of the Rocky mountains in the United States (Lilly and Zipser, 1972; Lilly, 1978) and the Yugoslavian bora in the mountains along the Adriatic coast of Yugoslavia (Smith, 1987) are two of the more famous and better documented of these winds. The Boulder windstorm is particularly strong with gusts as high as 60 m/s.

The early theories of Long (1953, 1954) and Houghton and Isaacson (1970) assumed that a pre-existing layering of the atmospheric stability was essential for the development of a severe wind state on the lee side of mountain ranges. Although a layered atmosphere may be a factor in the development of severe downslope winds, more recent numerical simulations of airflow over mountains by Clark and Peltier (1977), Peltier and Clark (1979), Durran (1986) and Bacmeister and Pierrehumbert (1988), hereafter CP77, PC79, D86 and BP88, respectively, have shown that a severe wind state can develop even when the mean wind speed and the stability are uniform with height as long as there is wave breaking aloft. These numerical simulations show that the onset of wave breaking leads to a re-organization of the flow field such that the downslope flow and associated drag can be much greater than that associated with the flow computed from linear theory or from steady nonlinear theory based on Long's equation (as described for example by Miles, 1969).

CP77 and PC79 were the first to discover the importance of wave breaking to the development of severe wind states. They hypothesized that the wave-breaking region aloft acted as a reflector of internal gravity waves (a "wave induced critical layer") and if this critical layer was near certain distinct heights H_0, a resonance would be established that eventually would lead to the re-organ-

* Present address: Universities Space Research Association, NASA/Goddard Space Flight Center, Greenbelt, MD 20771, USA.

ization of the flow into the severe wind state. Peltier and Clark (1983) developed a linear hydrostatic theory that predicts resonance will occur when $NH_0/U = \pi/2 + n\pi$, for $n = 0, 1, 2, \ldots$, where U is the (constant) wind speed below the critical layer and N is the buoyancy frequency. Their theory, being linear, implies that these critical heights are independent of the mountain amplitude.

In an attempt to verify their linear theory for resonance, Clark and Peltier (1984) performed a set of numerical experiments in which a zero-wind line was inserted into the initial flow at a prescribed height. This "environmental critical layer", as it is sometimes called, constrains wave breaking to occur at or just below the height of the zero-wind line, as long as the mountain's amplitude is small enough not to induce wave breaking without the presence of the critical layer. Clark and Peltier determined resonance heights by locating the peaks in the computed drag as a function of the height of the critical layer. They claimed that their numerical results supported the conclusions of their linear theory. However, further numerical experiments of this type by Durran and Klemp (1987) and BP88 showed that contrary to the linear theory the resonance heights are a function of the mountain amplitude and that a resonance is not achieved at all the heights where they are predicted to occur by the theory.

Another theory, developed by Smith (1985), hereafter S85, assumes that under some stratified conditions a region of well mixed turbulent air develops in the middle and upper troposphere above the mountain range. In other words, the existence of a wave-breaking region is assumed. Smith developed a nonlinear hydrostatic model of this flow for the case when the mean wind is shear free and the atmosphere is linearly stratified. The model has solutions that are easily computed and predicts the height of the well-mixed region, the speedup of the winds and the drag on the mountain range. This theory can be interpreted as a nonlinear generalization of Peltier and Clark's (1983) linear theory. The nonlinear theory predicts that resonance will occur at critical heights in the range $\pi/2 + n2\pi < NH_0/U < 3\pi/2 + n2\pi$, depending on the mountain amplitude. Note that for a particular mountain amplitude the nondimensional critical heights are separated by 2π whereas in the linear theory they are separated by π. The critical heights predicted by the nonlinear theory agree with all the numerical simulations described in the previous paragraph. Currently, this is the only theory for severe downslope winds that is consistent with the numerical simulations.

The present paper reports the results of flow visualization experiments in which we attempted to model severe downslope winds in a large stratified water channel. In all our experiments the fluid was linearly stratified and the mean flow upstream of the ridge was uniform. Three series of experiments were performed. In each series a different model ridge, each with a similar cross section but different streamwise aspect ratio, was used and the Froude number of the flow was varied over a range in which internal wave breaking was expected to occur. This is, we believe, the first systematic laboratory study of severe downslope winds, although many previous investigators have generated flows in the laboratory that resemble those presented here.

Our main objective was to test how well the numerical simulations of CP77, PC79, D86 and BP88 and the theory of S85 compare with real linearly stratified flows over obstacles. And in particular, to obtain some insight into how sensitive the conclusions about downslope winds based on these models are to small violations of their idealized flow assumptions.

Smith's theory produces no severe wind state solutions for mountain amplitudes that are higher than $0.985\,U/N$. Smith suggested, based on the experimental evidence of Snyder et al. (1985) and others, that the reason for this may be that for higher mountain amplitudes the flow upstream becomes blocked such that the *effective* mountain amplitude, the height above the blocked layer, is close to $0.985\,U/N$. Since in our experiments severe wind states were observed mostly for mountains higher than $0.985\,U/N$, we were able to test Smith's suggestions.

In Section 2 the experimental facilities and procedures are described. The results of the experiments are described in Section 3. The experimental results are compared with previous numerical simulations in Section 4. Section 5 contains a brief review of Smith's theory, including a more complete description of the extension of the theory to mountains higher than $0.985\,U/N$, and a comparison of our experimental results with the predictions of the theory. And in the final section our results are summarized and some conclusions are drawn.

2. Experimental procedure

The experiments were performed in the large stratified towing tank at the EPA Fluid Modeling Facility located in Research Triangle Park, North Carolina. The working section of the tank is 1.2 m deep, 2.4 m wide and 25 m long with side walls made of clear Plexiglas. Salt water with salt concentration varying in the vertical was used to produce the stratification. In all the experiments described here the density profiles were linear with a buoyancy frequency, $N=[-(g/\rho)\mathrm{d}\rho/\mathrm{d}z]^{1/2}$, of about 1.33 rad/s, where g is the acceleration due to gravity, and ρ is the fluid density. The specific gravity of the salt water varied from 1.2 at the bottom of the tank to 1.0 at the free surface. A more complete description of the towing tank and the methods used for producing and maintaining the density profile is given in Thompson and Snyder (1976), Hunt et al. (1978) and Hunt and Snyder (1980).

A towing carriage that travels on rails mounted on the side walls of the tank allows model obstacles to be towed along the length of the tank at speeds that can be varied between 2 cm/s and 50 cm/s. The ridges were mounted normal to the towing direction on a flat base plate and this whole apparatus was suspended upside down from the carriage and towed at the surface of the water with the base plate immersed about 0.5 cm. Although the model is towed in an inverted position the experiments will be discussed as though the model was in an upright position. The Froude number $F=U/NH$, where H is the ridge height, was varied by changing the tow speed U.

The ridges consisted of a spanwise length $2W$ of uniform cross section capped at both ends by a rotation of the cross-sectional profile through 180°. In all the experiments reported here the half-length W was 50 cm. The cross-sectional profile is given by the expression $z=(H/2)[1+\cos(\pi x/L)]$, where x is the horizontal coordinate in the streamwise direction measured from the crest of the ridge with $-L \leqslant x \leqslant L$. Three ridges were constructed out of molded Plexiglas or polystyrene foam with

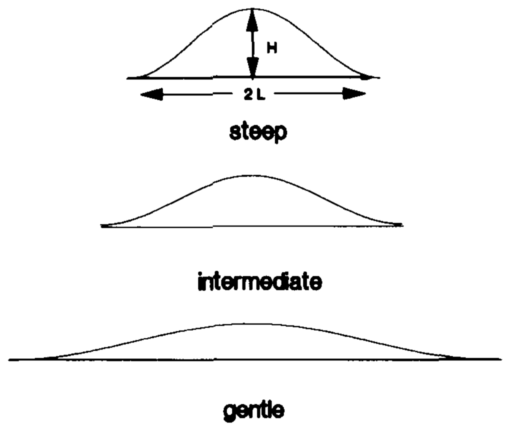

Fig. 1. The three ridge profiles drawn to scale.

$H/L=0.56$, 0.34 and 0.16, which are referred to as the steep, intermediate and gentle ridge. Table 1 lists the geometrical parameters for the three ridges. Fig. 1 shows the cross sectional shapes of the three ridges drawn to scale. The ridges were mounted on base plates that were either 240 cm by 250 cm or 240 cm by 275 cm with the ridge crest between 85 cm and 125 cm from the upstream edge of the base plate. A sketch of this arrangement is shown in Fig. 2.

The spanwise length of the ridges was chosen to make the flows as close to two dimensional as possible without causing the strong upstream effects demonstrated by Snyder et al. (1985). They showed that with ridges that spanned the entire width of the channel strong upstream columnar modes and flow blocking occurred when $F<1$, which result in a change in the vertical velocity and density profile upstream of the ridge. Furthermore, in a tank of finite length, the reflection of these columnar modes from the end wall produces continual changes in the upstream conditions so a steady state can never be achieved. Castro (1987) found experimentally that wave breaking never occurred steadily with ridges that spanned the whole width of the tank, but that breaking occurred intermittently and the location of the breaking waves changed during the tow. Based on the experience of Snyder et al. (1985), we chose the spanwise length of the ridges to be as long as is possible without producing continual upstream changes. Since the ridges span only 40% of the channel width, some fluid is allowed to flow around the ridges rather than

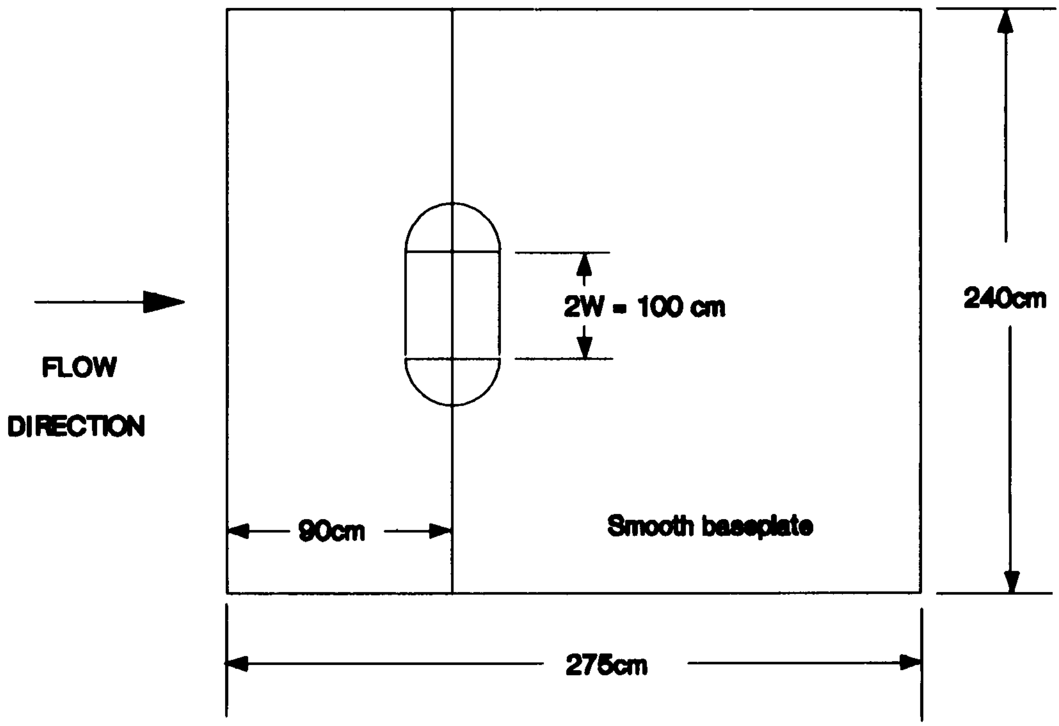

Fig. 2. A plan view of the steep ridge mounted on the base plate.

forcing all the fluid over them. The flow near the center of the ridge remains nearly two dimensional, complete with blocked flow when $F < 1$; only the unsteadiness of the upstream conditions has been minimized by allowing some fluid to flow around the ridges.

The streamwise aspect ratio of the gentle ridge was chosen to be as small as was physically reasonable in the tank, yet its slope is steeper than most real mountain ranges. The streamwise aspect ratios of the steep and intermediate ridges were chosen in an attempt to study how far the hydrostatic assumption of the theory to be described in Section 5 could be pushed.

Clearly, flow separation on the lee of the ridges will significantly affect the strength of downslope flows. Separation depends on the steepness of the ridge, the Reynolds number and the Froude number. Since we are attempting to simulate atmospheric flows, we would like to minimize the Reynolds number dependence. The Reynolds number based on the ridge height, Re, for the experiments described here was in the range $800 < \text{Re} < 13{,}000$. Lee et al. (1987), who used the same ridges as we used in the present experiments, found that in neutral flow over the steep ridge separation always occurred and the point of separation was always near the ridge crest. However, in neutral flow over the intermediate and gentle ridges separation occurred at the low end of the Re range but not at the high end. To eliminate this Reynolds number dependence, the intermediate and gentle ridges and their base plates had their surfaces roughened by a covering of 4 mm diameter (average) gravel with an average distribution of about 30 stones per 100 cm^2. This was an attempt to create a turbulent boundary layer for all Re used in our experiments. In addition a 5 mm boundary layer trip was added at the crests of the intermediate and gentle ridges to force separation under neutral conditions to occur near the crest. These changes were found to eliminate the Reynolds number dependence of the lee separation under neutral conditions, although in effect we have made the gentle ridge steeper than it really is by forcing the separation to occur at the crest.

The flow was visualized by emitting dye

plumes at various positions near the models. An acid powdered dye was mixed with the proper concentration of salt water so that the mixture was neutrally buoyant at the level at which it was released. Usually several plumes at 2 cm intervals were emitted from a vertical rake of tubes mounted on the centerline at the upstream edge of the base plate. The tips of these tubes were bent-over 90° toward the model. The number of plumes and their vertical positions were varied depending on the anticipated nature of the flow. If the flow is steady, or nearly so, the paths of these plumes correspond to streamlines. Each experiment was recorded on video tape and on 35 mm color slide film. The video camera and still camera were mounted on one side of the tank and towed along with the model carriage.

3. Results and discussion

3.1. Preliminary considerations

Based on the ideas discussed in the introduction, wave breaking is critical to the development of a severe downslope wind state. Therefore, we need to estimate the range of the flow parameters in our experimental arrangement for which wave breaking will occur. The three independent dimensionless parameters of importance that were varied in these experiments were: the streamwise aspect ratio H/L, the spanwise aspect ratio H/W and the Froude number $F = U/(N/H)$. The values of H/L and H/W have already been fixed as described in the previous section. To estimate the range of F as a function of H/L and H/W for which wave breaking will occur for each ridge, we turn to some previous theoretical and experimental work on breaking lee waves for guidance.

Huppert and Miles (1969) solved Long's equation for steady nonlinear lee waves over a two-dimensional obstacle with a semi-elliptical cross section for values of the streamwise aspect ratio that varied from $H/L = \infty$ (a vertical strip) to $H/L = 0$ (the hydrostatic limit). They were able to compute the value of the critical Froude number, F_c, at which the flow first becomes statically unstable at some point (a vertical streamline appears at one point in the flow). When $F > F_c$ Long's model produces smooth steady lee waves over the obstacle and when $F < F_c$ it produces streamlines that overturn (which violates the assumptions on which Long's model is based). Presumably, this means that wave breaking occurs when $F < F_c$. Their calculations show that F_c increases monotonically from 0.58 for $H/L = \infty$ to 1.49 for $H/L = 0$. Although these values are somewhat dependent on the hill cross section (for example Miles and Huppert (1969) show that $F_c = 1.18$ when $H/L = 0$ for a *witch of Agnesi* hill), they give us a good approximate range of F for which to look for breaking internal waves.

Castro (1987) performed a series of laboratory experiments in which he explored how lee wave breaking depended on the spanwise aspect ratio of an obstacle of fixed streamwise aspect ratio. The upstream flow conditions in his experiments were just as they are in our experiments; in fact, his experiments were done in the same tank. The obstacle he used had a triangular cross section with a streamwise aspect ratio of $H/L = 2.0$. Castro observed that F_c increased monotonically from about 0.4 for $H/W = 6.0$ to about 1.0 for $H/W = 0$. Beyond $H/W = 6.0$ no wave breaking was observed at any Froude number. Generally, wave breaking was observed for values of F such that $F_c > F > 0.2$. The observed value of F_c at $H/W = 0$ (the two dimensional limit) for a triangular shaped ridge is fairly close to the value predicted by Huppert and Miles (1969) for a semi-elliptically shaped ridge with $H/L = 2.0$.

Therefore, apparently F_c increases as either the streamwise aspect ratio or the spanwise aspect ratio decreases. From the geometrical data in Table 1, both of these ratios decrease together as we progress from the steep ridge through the

Table 1. *Geometric parameters for the ridges, where H is the ridge height, L is the streamwise half-length of the ridge and W is the spanwise half-length*

Ridge model	H (cm)	L (cm)	W (cm)	H/L	H/W	Maximum slope
steep	10.4*	18.5	50.0	0.56	0.20	40°
intermediate	7.5†	22.0	50.0	0.34	0.15	27°
gentle	5.8†	35.5	50.0	0.16	0.12	13°

* Includes 0.4 cm step where model is fastened to base plate.

† Includes 0.5 cm boundary layer trip at ridge crest.

intermediate ridge and to the gentle ridge. It appears that if we vary F such that $1.5 > F > 0.2$ then we should cover all the possible conditions when breaking waves will occur for the three ridges used in our experiments and the value of F_c should increase as the steepness of the ridges decreases.

3.2. *Wave breaking*

Selected photographs of the flows are shown in Figs. 3–5 for the steep, intermediate and gentle ridge, respectively, for several values of the Froude number. These photographs were taken when the ridge had been towed about half-way down the length of the tank, a sufficient distance for a steady state to have been established.

For the steep ridge, wave breaking and the formation of a well-mixed region was observed when $F = 0.2$, 0.3, 0.4, 0.5 and 0.6. When $F = 0.7$ and 0.8, wave breaking occurred intermittently during the tows and when $F = 0.9$ there was no evidence of wave breaking. For the intermediate ridge, wave breaking was observed when $F = 0.2$, 0.3, 0.4, 0.5, 0.6 and 0.7. When $F = 0.8$ and 0.9, wave breaking appeared intermittently and when $F = 1.0$ there was no wave breaking at all. For the gentle ridge, wave breaking was observed when $F = 0.2$, 0.3, ..., 0.95. Wave breaking appeared toward the end of the tow when $F = 1.0$, but this should probably be disregarded as due to end effects in the tank. For larger values of F no wave breaking was observed. Continuous wave breaking was observed for this ridge in some earlier preliminary experiments (Rottman and Smith, 1987) when $F = 1.1$ and it was not until $F = 1.2$ that wave breaking became intermittent. The gentle ridge had the smallest height of the three ridges and it is close to the free surface where the density profile is most distorted from a linear gradient, so the accurate determination of the Froude number is most difficult for this ridge. We feel that the present measurements are more accurate than the previously published results due to the care taken in the preparation of the present experiments, but it should be kept in mind that there is a possible error of about 0.1 in the measurement of the Froude number for the gentle ridge. Table 2 lists the experiments we performed and identifies those for which wave breaking was observed.

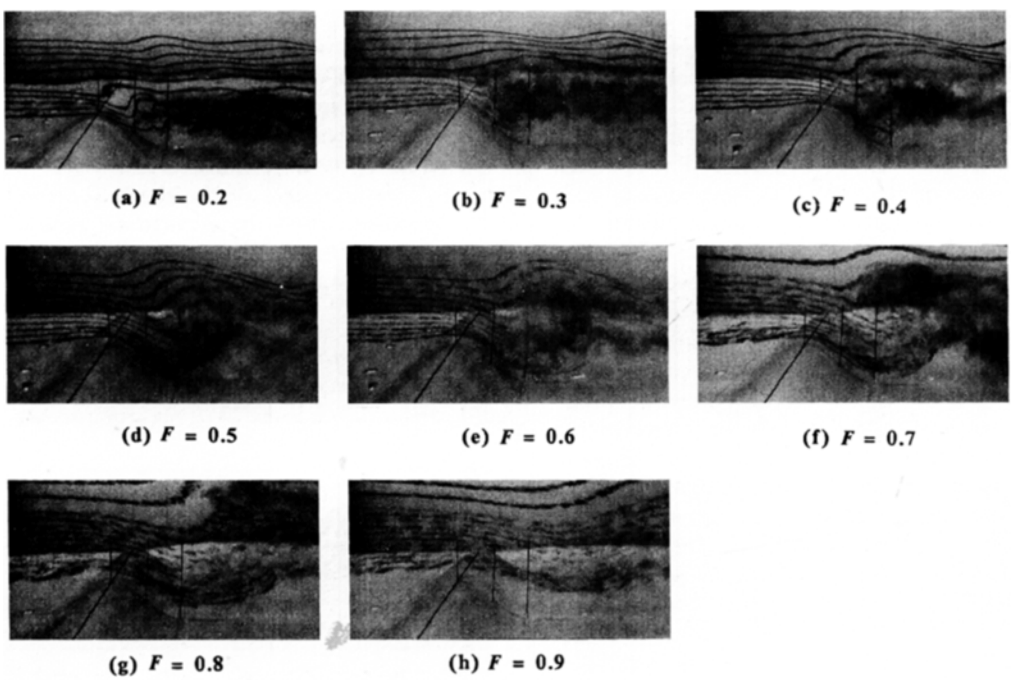

(a) $F = 0.2$ (b) $F = 0.3$ (c) $F = 0.4$

(d) $F = 0.5$ (e) $F = 0.6$ (f) $F = 0.7$

(g) $F = 0.8$ (h) $F = 0.9$

Fig. 3. The flow over the steep ridge at several Froude numbers.

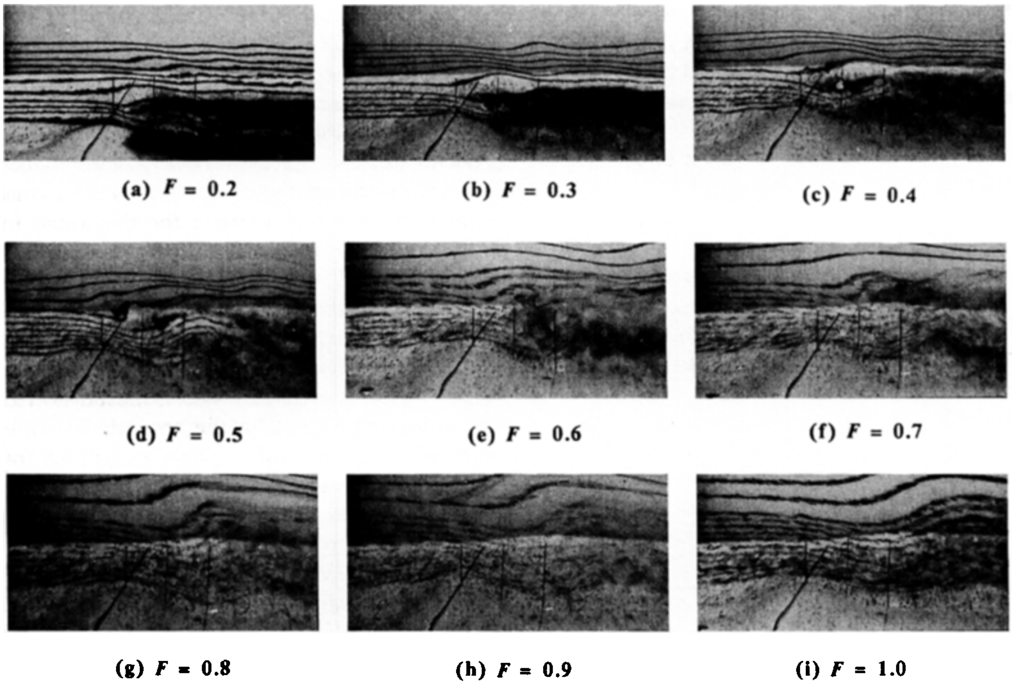

Fig. 4. The flow over the intermediate ridge at several Froude numbers.

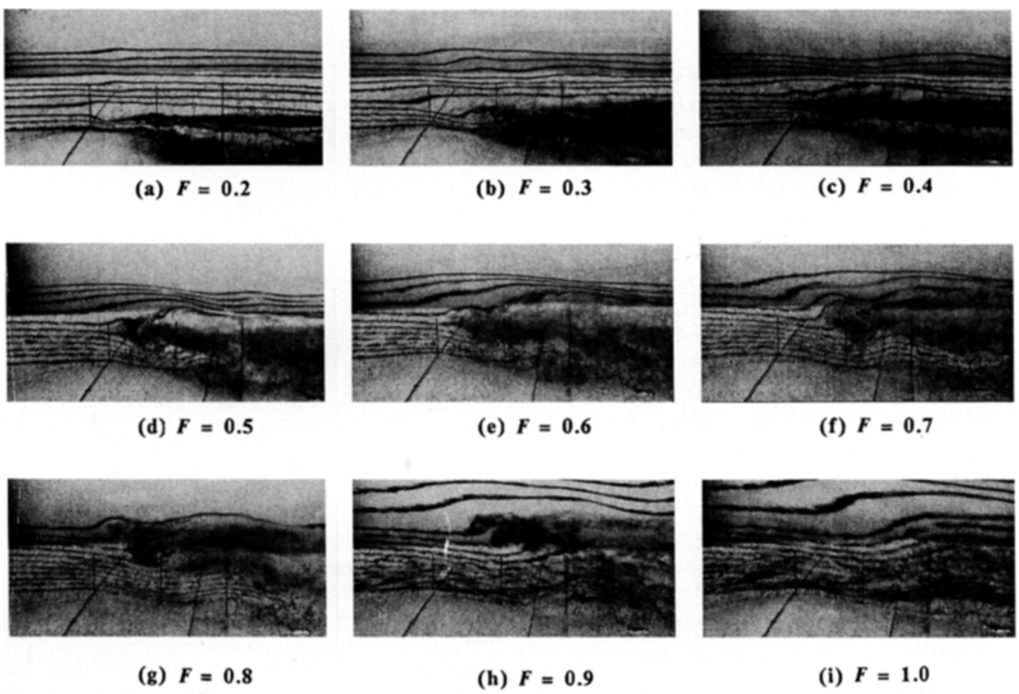

Fig. 5. The flow over the gentle ridge at several Froude numbers.

Table 2. *A list of the experiments performed, indicating in which wave breaking was observed: B, continuous wave breaking observed; I, intermittent wave breaking observed; N, no wave breaking observed*

F	Steep ridge	Intermediate ridge	Gentle ridge
0.2	B	B	B
0.3	B	B	B
0.4	B	B	B
0.5	B	B	B
0.6	B	B	B
0.7	I	B	B
0.8	I	I	B
0.9	N	I	B
0.95	*	*	B
1.0	*	N	I
1.1	*	*	N
1.2	*	*	N
1.45	*	*	N

* No experiment performed for this value of F.

We conclude from these observations that $F_c = 0.8$, 0.9 and 1.0 for the steep, intermediate and gentle ridge, respectively. These results for wave breaking are consistent with the estimates made earlier based on the theoretical predictions of Huppert and Miles (1969) and the previous experimental work of Castro (1987). It appears from the photographs that the region of mixed fluid produced by wave-breaking is small for the smaller values of the Froude number and becomes increasingly larger as the Froude number increases until the critical Froude number is reached at which wave breaking ceases to occur. This well-mixed region was maintained by continual wave breaking. When wave breaking was intermittent the well-mixed region disappeared between the episodes of wave breaking.

The distortion of the dye plumes above the wave breaking region shows that there is a substantial amount of energy being propagated vertically away from this region by lee waves. This indicates that the wave breaking region is far from being a perfect reflector of wave energy.

3.3. *Measurement of the height of the wave-breaking region*

We attempted to measure the height H_0 of the wave-breaking region when it existed. The measurements were made directly from digitized video images of the tows. To be consistent with the definition used in Smith's theory, we defined H_0 as the upstream height above the base plate of the streamline that marks the top of the wave breaking region. Since the dye plumes in our experiments are spaced every 2 cm, we of course could not resolve H_0 with any more accuracy than that. The measured values of the nondimensional height $\hat{H}_0 = NH_0/U$ are plotted in Fig. 6 along with the values obtained from numerical simulations and Smith's theory, which will be described in more detail later. The measured values of $\hat{H}_0$ increase as F decreases for each of the ridges. In fact, $\hat{H}_0$ roughly doubles as F decreases from F_c to 0.2. There is a small but consistent decrease in $\hat{H}_0$ as the steepness of the ridges increases. We emphasize that these measurements are somewhat subjective, as it is difficult to see accurately the shape of the region in the video images. However, by making several measurements we are fairly confident that the trends of the data are reproducible.

It appears from our observations plotted in Fig. 6 that the eventual height of the wave breaking region, whenever it existed continuously in our experiments, is close to the critical height predicted by Smith's theory. Thus, based on the theory, we would expect a severe downslope wind state to exist in our experiments whenever a wave breaking region existed above the ridge.

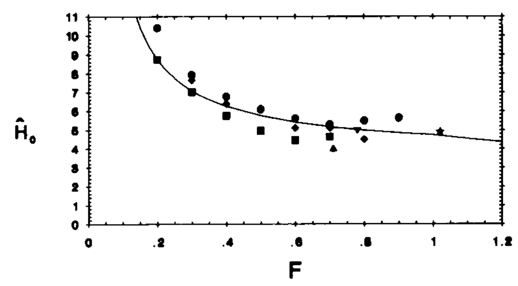

Fig. 6. A plot of the nondimensional critical streamline height $\hat{H}_0$ as a function of the Froude number. Experimental measurements: ■, steep ridge; ◆, intermediate ridge; ●, gentle ridge. Numerical simulations: ▼, Peltier and Clark (1979); ▲, Durran (1986); ★, Bacmeister and Pierrehumbert (1988). Theory: ——, eq. (5.2).

3.4. Measurement of the downslope flow speed

In the numerical simulations described in the introduction, a severe wind state was defined by a large increase in the drag and in the downslope surface wind speed over that expected from linear or nonlinear steady theory based on Long's equation. In our experiments, it is very difficult to measure accurately the drag on the ridges (although we did attempt to measure the drag unsuccessfully), so we have only the downslope surface wind speed as a measure of the existence of a severe wind state.

We used digitized video images of the tows to measure the velocity on the downstream side of the ridge. The position of blobs of dye in the dye plumes were measured and tracked over several frames of the video tape. This enabled an average speed to be computed for each blob over a short distance. We made these measurements for several dye plumes to produce a velocity profile for the flow near the ridge surface on the downstream side of the ridge along the centerline.

The main point of interest here is the ratio of the maximum speed of the downslope flow to the upstream mean flow speed; these values are plotted in Fig. 7, along with the values obtained from numerical simulations and Smith's theory. Without the presence of a wave-breaking region a speedup of about 1.5 was measured. With wave breaking, the measurements show that the speedup is between about 2.0 and 2.5. Although the downslope flow is clearly stronger with the presence of a wave-breaking region than without it, the speedup, as shown in Fig. 7, is less than would be expected based on the results of numerical simulations and Smith's hydrostatic theory. Apparently some physical effect in the experiments is not accounted for in the numerical simulations nor in the theory.

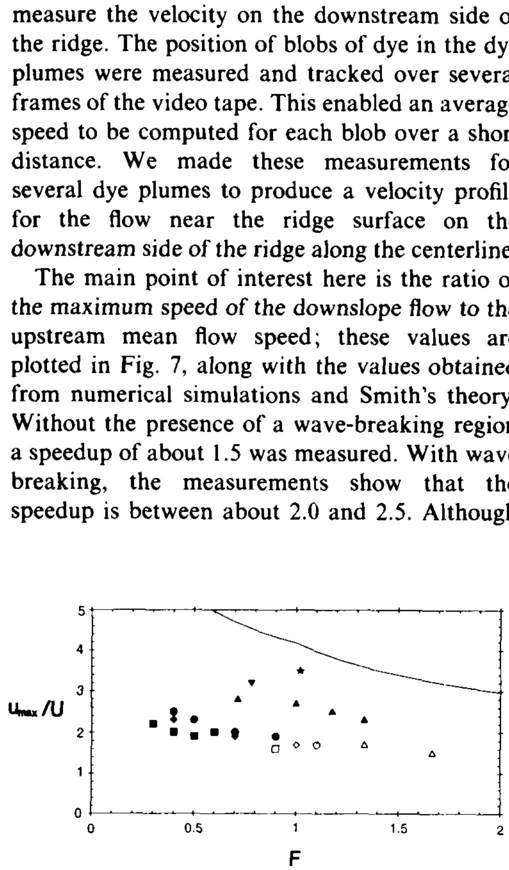

Fig. 7. A plot of the nondimensional maximum surface downslope windspeed as a function of the Froude number. Experimental measurements: ■, steep ridge; ◆, intermediate ridge; ●, gentle ridge. Numerical simulations: ▼, Peltier and Clark (1979); ▲, Durran (1986); ★, Bacmeister and Pierrehumbert (1988). Theory: ——, eq. (5.5). A solid symbol indicates that wave breaking was present and an open symbol that it was not.

3.5. Separation on the lee of the ridges

An important influence on the existence of the severe wind state is where the flow separates, or whether the flow separates at all, on the lee side of the ridge. Separation will increase the turbulence near the surface and decrease the mean tangential flow speed. The numerical simulations described briefly in the introduction and in more detail in the next section do not properly account for separation.

The experiments of Hunt and Snyder (1980) on stably stratified flow over three-dimensional hills provide some guidance on this point. They showed that lee side separation in stably stratified flows is determined by the parameter $\lambda/2L$, where $\lambda = 2\pi U/N$ is the fundamental lee wave wavelength in a vertically unbounded fluid domain. When $\lambda/2L \gg 1$, the over the hill is like that of neutral flow; that is, separation is controlled by the pressure field in the boundary layer over the ridge. For the present case, this means that the flow separates near the crest. When $\lambda/2L$ is of order unity, separation is determined by the pressure field associated with the lee waves. When $\lambda/2L \approx 1$, the lee wave closely matches the contour of the hill and separation is completely suppressed. When $\lambda/2L < 1$, separation occurs at the location of the trough of the first lee wave; that is, the separation point is located at $x_s \approx \frac{1}{2}\lambda$, where x_s is the horizontal distance downstream from the ridge crest to the separation point. The value of $\lambda/2L$ for each experiment we performed is listed in Table 3.

The photographs in Figs. 3–5 show that the flow does separate on the lee side of the ridge when $\lambda/2L < 1$ and that separation is suppressed when $\lambda/2L \approx 1$. Although it is difficult to measure the separation point with any accuracy, we estimated the position of the separation point from the averaged streamline plots and found that $x_s \approx \frac{1}{2}\lambda$ is a fairly good description of

Table 3. *The value of the parameter $\lambda/2L$ for each experiment, where $\lambda = 2\pi U/N$*

	$\lambda/2L$		
F	Steep ridge	Intermediate ridge	Gentle ridge
0.2	0.35	0.21	0.10
0.3	0.52	0.32	0.15
0.4	0.70	0.43	0.21
0.5	0.87	0.53	0.26
0.6	1.05	0.64	0.31
0.7	1.22	0.75	0.36
0.8	1.40	0.85	0.41
0.9	1.57	0.96	0.46
0.95	*	*	0.49
1.0	*	1.06	0.52
1.1	*	*	0.57
1.2	*	*	0.62
1.45	*	*	0.74

* No experiment performed for this value of F.

our measurements when $\lambda/2L < 1$. That is, it appeared as if the lowest dye plume turned upward from the lee slope where $0.4\lambda < x_s < 0.8\lambda$, when $\lambda/2L < 1$. Some other technique must be used to measure this with any more accuracy.

4. Comparison with numerical simulations

Three numerical studies of downslope winds reported in PC79, D86 and BP88 were done under conditions similar enough to our laboratory experiments that a reasonable comparison can be made. In each of these studies the upstream mean flow and stability were uniform, just as in our experiments, and the ridges used were two-dimensional with a *witch of Agnesi* cross section ($z = H/[1 + x^2/D^2]$, where D is the half-width of the ridge surface when $z = H/2$), not the same but similar enough to our experiments for a reasonable comparison. All of these studies used finite-difference schemes to obtain a numerical solution of the two-dimensional equations of motion for large Reynolds number flow, with a free-slip boundary condition on the ridge surface. The effects of turbulence on the mean flow were approximated by first-order closure schemes.

In Section 4 of PC79 the results of one numerical simulation is reported in detail in which $F = 0.78$ and $H/D = 0.17$. The streamwise aspect ratio H/D is close to that of our gentle ridge (although there is no direct analog to L for the *witch of Agnesi* ridge), and the value of F puts this simulation, based on our experimental results, in the strong wave breaking regime. The numerical simulations were initiated in essentially the same way as in our experiments; that is, by accelerating the flow from rest to a constant speed over some small time. The calculations were not continued to a complete steady state, but were stopped at about the time wave breaking began. For this particular calculation the turbulence model was turned off, although the main results are nearly the same as described in CP77 in which the same calculation was made with the turbulence model turned on.

Both the surface drag and the maximum surface wind in the calculation increased linearly with time. When the calculation was terminated, the upstream height of the streamline that first became vertical was about $NH_0/U = 5.0$ and the ratio of the maximum surface wind speed to the mean upwind speed u_{max}/U was about 3.2 (the linear theory value for this quantity is 1.64). These values are plotted in Figs. 6 and 7, respectively.

In Section 6 of D86, numerical calculations similar to those of CP77 and PC79 except carried further in time, closer to a steady state, are described. Apparently simulations were made for 6 values of F ranging from 0.71 to ∞. Since the ridge half-width was fixed and the ridge height varied to change the Froude number, the streamwise aspect ratio H/D was different in each calculation, varying from 0.14 to 0, respectively.

The streamline plot shown in Fig. 16d of D86, for the case with $F = 0.71$ and $H/D = 0.14$ (the only case for which a streamline plot is presented), is qualitatively similar to our Fig. 5f, if account is taken for the exaggerated vertical scale in D86. The most important difference is that the laboratory experiments show some separation at the base of the lee slope of the ridge that does not appear in the computed streamline pattern. From the plot in D86, we estimate the level of the wave breaking region to be $NH_0/U = 4.0$. This value is plotted in Fig. 6 and the values of u_{max}/U for all 6 cases are plotted in Fig. 7.

In Section 4 of BP88, two numerical calculations for which $F = 1.02$ and $H/D = 0.098$ and

$F = 2.0$ and $H/D = 0.05$ are described. These calculations were initiated with the flow produced from S85's ideal high drag state (as sketched in Fig. 8 of the present paper). For the case with $F = 1.02$, the flow remained essentially in the high drag state as the calculations progressed in time, whereas in the $F = 2.0$ case the flow relaxed to that expected from Long's model. This is the anticipated result since, for the streamwise aspect ratios of the ridges in these calculations, we would expect wave breaking to occur for $F = 1.02$ but not for $F = 2.0$.

From the streamline pattern for the $F = 1.02$ case, Fig. 12 in BP88, we measured $NH_0/U = 4.9$, which is plotted in Fig. 6. The value of u_{max}/U reported for this case is 3.5, which is also plotted in Fig. 7. We cannot compare the streamline pattern in Fig. 12 directly with any of our experiments, since for the streamwise aspect ratios in our experiments wave breaking did not occur for this value of F. However, the flow pattern in Fig. 12 is clearly qualitatively similar to our Fig. 5g, when the scale differences are taken into account. It is concluded in BP88 that continuous wave breaking is required to maintain the severe wind state and that a substantial amount of energy is transported vertically away from the wave breaking zone. These observations are completely consistent with our experimental observations.

In summary, the numerical simulations do a fairly good job of describing our laboratory experiments. The breaking region, when it exists, is calculated to have approximately the same shape as in our experiments and the computed height of the breaking region as shown in Fig. 6, is very consistent with our measured height. The main discrepancy is the strength of the downslope flow; in general the numerical simulations have larger downslope flows than we measured in the laboratory, as shown in Fig. 7. Two obvious reasons the experimental values are lower than the numerical simulations is the existence in the laboratory of a turbulent boundary layer and the possibility of separation on the lee of the ridges. (The numerical models all use a free-slip boundary condition at the hill surface.) Another reason the experimentally measured values of the speedup ratio are lower than expected is that the measurement technique we used averages the speed over about half the distance from the crest to the ridge base on the lee side of the ridge. Since the numerical simulations indicate that the tangential surface speed peaks rather sharply on the lee side of the crest, it is not surprising that our measured values for the speed are somewhat lower than the computed maxima.

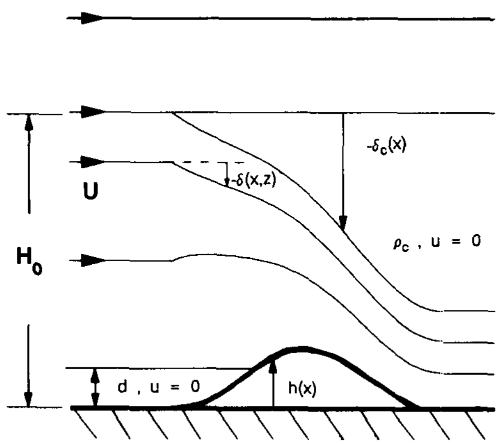

Fig. 8. A schematic of the idealized severe wind state configuration as hypothesized by Smith (1985). The upstream fluid speed U is uniform and the upstream density gradient is linear with buoyancy frequency N. The upstream flow has been modified by a blocked layer of depth d, where $d = 0$ when $NH/U < 0.985$ and $d = H - 0.985U/N$ when $NH/U > 0.985$.

5. Comparison with the theory of Smith

Fig. 8 shows a sketch of the idealized severe downslope wind configuration hypothesized in S85, in which the ridge is centered at the origin of a coordinate system with x as the horizontal coordinate as z as the vertical coordinate. Far upstream of the ridge the flow has uniform speed U with constant buoyancy frequency N. Over the ridge there is an intrusion consisting of stagnant but well-mixed fluid of density ρ_c. The critical streamline that splits to go around this intrusion originates upstream at the height $z = H_0$. Above H_0, the flow is undisturbed. Below the streamline that is the lower boundary of the intrusion the flow is assumed to be described by the hydrostatic version of Long's (1955) equation for a Boussinesq fluid. The boundary conditions for the solution of Long's equation in this lower region are $\delta(x, h) = h(x)$ on the lower surface

$z = h(x)$, where $\delta(x, z)$ is the vertical displacement of a streamline from its upstream height, and $\delta_z = 0$ on the streamline bounding the intrusion $z = H_0 + \delta_c(x)$, where $\delta_c(x)$ is the vertical displacement of the critical streamline from H_0.

With these assumptions the vertical displacement $\delta_c(x)$ of the critical streamline is the solution of

$$\hat{h} = \hat{\delta}_c \cos(\hat{H}_0 + \hat{\delta}_c - \hat{h}) \quad (5.1)$$

for a specified ridge profile $\hat{h}(x)$. A circumflex ^ over a quantity means that the quantity is nondimensionalized with the length scale U/N. Fig. 9 is a plot of $\hat{\delta}_c$ as a function of $\hat{h}$ that satisfies (5.1), for several specified values of $\hat{H}_0$. Note that for a given $\hat{H}$, the maximum ridge height, there is only one value of $\hat{H}_0$ (except for values that differ from $\hat{H}_0$ by an integer multiple of 2π, which have the same solution curve) for which there is a transitional flow over the ridge; that is, only one value of $\hat{H}_0$ will produce a permanent displacement of the critical streamline, which is associated with the severe wind state, for a given maximum ridge height. These solutions for "positive" ridges are the curves in the fourth quadrant.

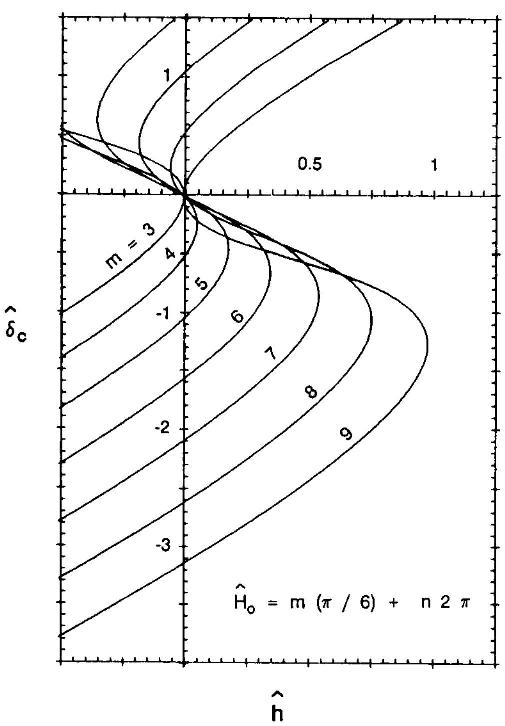

Fig. 9. Solution curves for eq. (5.1). Each curve is for a different value of the critical streamline height $\hat{H}_0$. The curves in the 4th quadrant represent transitional flows over positive ridges, like the flow illustrated in Fig. 8.

The critical streamline height $\hat{H}_0$ is given by the expression

$$\hat{H}_0 = \hat{H} - \hat{\delta}_{cm} + \arccos(\hat{H}/\hat{\delta}_{cm}) + n2\pi, \quad (5.2)$$

where $n = 0, 1, 2, \ldots$ and

$$\hat{\delta}_{cm} = -[\hat{H}^2/2 + \hat{H}(\hat{H}^2 + 4)^{1/2}/2]^{1/2}, \quad (5.3)$$

(Smith and Sun, 1987). This expression is valid for positive mountains with $0 < \hat{H} \leqslant 0.985$ although for $\hat{H} < 0.67$, say, there may be no mechanism (such as wave breaking) in a time dependent flow to initiate a re-organization into a severe wind state. The theory has no transitional solutions for $\hat{H} > 0.985$, although numerical simulations and our experiments show that a severe wind state generally exists for $\hat{H} > 0.985$.

Smith suggests that in this case a blocked layer exists upstream of the ridge, as shown in Fig. 8, such that the *effective* ridge height $\hat{H}_{\text{eff}}$, the height of the ridge crest above the blocked layer, is near 0.985; that is, the blocked layer has a depth $\hat{d} = \hat{H} - 0.985$ when $\hat{H} > 0.985$. This idea is consistent with the extensive observations of Snyder et al. (1985) and others who found that stably stratified flow around three-dimensional obstacles is essentially horizontal below the height $\hat{d}$ meaning that the flow below $\hat{d}$ goes around the ridge instead of over it. Substituting $\hat{H}_{\text{eff}} = 0.985$ for $\hat{H}$ in (5.2) and (5.3), we get $\hat{H}_{0\,\text{eff}} = 3\pi/2 + n2\pi$ as the upstream height of the critical streamline *above* the blocked layer and therefore

$$\hat{H}_0 = 3\pi/2 + \hat{d} + n2\pi \quad (5.4)$$

for all $\hat{H} > 0.985$.

$\hat{H}_0$ given by (5.2) and (5.4) (with $n = 0$) is plotted as a function of $F = 1/\hat{H}$ in Fig. 6 along with our experimental measurements of the height of the wave breaking region and estimates of $\hat{H}_0$ from the numerical simulations. As noted previously, the agreement is very good. We comment here that when $\hat{H} = 0.985$ both the linear theory of Peltier and Clark (1983) and the nonlinear theory of S85 give the same value for

$\hat{H}_0 = 3\pi/2$, although for smaller values $\hat{H}$ they give different results. Thus, since $\hat{H}_{eff} = 0.985$ in all of our experiments, our results cannot be used to distinguish between the two theories if in both we incorporate the idea of a blocked layer of depth d. (The numerical calculations of Durran and Klemp (1987) and BP88 seem to be best suited for this purpose and as noted in the introduction are consistent with the theory of S85).

The maximum speedup ratio u_{max}/U can also be computed from the theory. If we let $\delta_{c\,max}$ be the value of δ_c as $x \Rightarrow \infty$ for transitional flow over the ridge, then

$$u_{max}/U = 1 - \hat{\delta}_{c\,max}. \tag{5.5}$$

When $\hat{H} < 0.985$, then $\hat{\delta}_{c\,max}$ is the value of $\hat{\delta}_c$ at $\hat{h} = 0$ in (5.1); that is, $\hat{\delta}_{c\,max} = \pi/2 - \hat{H}_0$ with $\hat{H}_0$ given by (5.2). When $\hat{H} \geqslant 0.985$, the situation is complicated by the existence of the blocked layer upstream of the ridge. In this case $\hat{\delta}_{c\,max}$ is the value of $\hat{\delta}_c$ at $\hat{h} = -\hat{d} = 0.985 - \hat{H}$ in (5.1), which must be determined numerically.

The values of u_{max}/U computed as described above are plotted in Fig. 7 as a function of $F = 1/H$ along with the previously described experimental and numerical results. As seen from the plot, the theory over-predicts the speedup ratios compared with the experiments and with the numerical simulations, although the latter are closer to the theory than the former. As mentioned previously, two reasons the experimental values for the downslope flow are so much lower is the existence in the laboratory of a turbulent boundary layer and the possibility of separation on the lee of the ridges. The effect of a separated flow may be partially accounted for in the theory by defining $\delta_{c\,max}$ as the value of δ_c at $\hat{h}$ where separation occurs. This will reduce the value of u_{max}/U, but it is somewhat difficult to apply in the context of a hydrostatic theory when the separation point is a function of H/L.

Finally, the shape of the wave-breaking region assumed by S85 and sketched in Fig. 8 is in some important ways not quite what is observed in the experiments. The observed well-mixed region, created and maintained by continuously breaking lee waves, always appears downstream of the ridge and is generally greatly distorted by the lee waves, whereas the theoretical well-mixed region begins as a sharp wedge at the upstream base of the ridge and extends downstream with a flat upper boundary. In addition, as already noted, the flow above the well-mixed region was always observed to be disturbed by large amplitude lee waves, whereas S85 assumes that the flow above the well-mixed region is undisturbed. That is, S85 assumes the well-mixed region to be a perfect reflector of internal waves, which apparently is not the case.

These observations about the strength of the downslope flow, the shape of the well-mixed region and the flow aloft are probably all related and suggest that the upper boundary condition in S85, while possibly a useful first approximation, needs to be modified to explain some important details of the flow.

6. Summary and conclusions

We have found experimentally that in linearly stratified flow over a ridge a well-mixed region of turbulent field, created and maintained by breaking lee waves, forms in the lee of the ridge over a range of Froude numbers that is a function of the ridge steepness. This range of Froude numbers was measured to be $0.2 < F < F_c$, where $F_c = 0.8$, 0.9 and 1.0 for the steep, intermediate and gentle ridge, respectively.

The measured values for H_0, the upstream height of the streamline that marks the top of the well-mixed region (when such a region existed), were shown to compare very well with the values that correspond to a severe downslope wind state as predicted by the theory of S85, although there was a slight trend for $\hat{H}_0$ to decrease as the steepness of the ridge increased. The measured values of H_0 also compared well with the results of previous numerical simulations which exhibited severe downslope winds.

However, although the measured velocity profiles on the downstream side of the ridges showed a definite speedup in the presence of a well-mixed region aloft, the speedup tended to be weaker, based on the previous numerical simulations and the theory of S85, than would be expected in a severe downslope wind state. Possible physical reasons for this discrepancy are the presence of a boundary layer near the surface and flow separation on the lee side of the ridge, which are not present in the numerical simulations nor in the theory. Another possibility is that our measurement technique was not precise enough to measure the maximum speedup, which the numerical simulations indicate tended to peak sharply downstream of the ridge crest.

We conclude that the numerical simulations do a very good job of describing severe downslope wind states generated by the flow of real stratified fluids over a ridge, although this conclusion is based on a rather small number of numerical simulations. Another difficulty for these two-dimensional numerical models can be foreseen when calculations are made for small Froude numbers. In this case strong upstream effects will be generated and the upstream boundary conditions will have to be treated very carefully.

Based on our laboratory experiments and previous numerical simulations, we conclude also that, although not perfect, the nonlinear hydrostatic theory of S85 apparently captures the essential mechanism of severe downslope winds. The deficiencies in the theory may be related to the upper boundary condition, in which the flow above the well-mixed region is assumed to be undisturbed. The results of our experiments show that a significant amount of energy escapes the flow below the well-mixed region and is propagated vertically by lee waves. This may account in part for the theory's over prediction of the strength of the downslope flow as compared with both the numerical simulations and our laboratory experiments. These observations indicate that the upper boundary condition in S85 needs to be modified to explain some details of the flow.

7. Acknowledgements

We thank J. T. Lee for allowing us access to some of his data and for many useful technical discussions. We also thank for their help the entire staff at the US Environmental Protection Agency's Fluid Modeling Facility and in particular R. E. Lawson, Jr., G. L. Marsh, and W. H. Snyder. The work reported in this paper was supported by the US Environmental Protection Agency through the Cooperative Agreement CR-811973 with North Carolina State University.

REFERENCES

Bacmeister, J. T. and Pierrehumbert, R. T. 1988. On high drag states of nonlinear stratified flow over an obstacle. *J. Atmos. Sci. 45*, 63–80.

Castro, I. P. 1987. A note on lee wave structures in stratified flow over three-dimensional obstacles. *Tellus 39A*, 72–81.

Clark, T. L. and Peltier, W. R. 1977. On the evolution and stability of finite amplitude mountain waves. *J. Atmos. Sci. 34*, 1715–1730.

Clark, T. L. and Peltier, W. R. 1984. Critical level reflection and the resonant growth of nonlinear mountain waves. *J. Atmos. Sci. 41*, 3122–3134.

Durran, D. R. 1986. Another look at downslope windstorms. Part I: The development of analogs to supercritical flow in an infinitely deep, continuously stratified fluid. *J. Atmos. Sci. 43*, 2527–2543.

Durran, D. R. and Klemp, J. B. 1987. Another look at downslope winds. Part II: Nonlinear amplification beneath wave-overturning layers. *J. Atmos. Sci. 44*, 3402–3412.

Houghton, D. D. and Isaacson, E. 1970. Mountain winds. *Studies in Numerical Analysis 2*, 21–52.

Hunt, J. C. R. and Snyder, W. H. 1980. Experiments on stably and neutrally stratified flow over a model three-dimensional hill. *J. Fluid Mech. 96*, 671–704.

Hunt, J. C. R., Snyder, W. H. and Lawson, R. E., Jr. 1978. Flow structure and turbulent diffusion around a three-dimensional hill: Fluid modeling study on effects of stratification; Part 1. Flow structure. *USEPA Rep. EPA-600/4-78-041*, Research Triangle Park, North Carolina.

Huppert, H. E. and Miles, J. W. 1969. Lee waves in a stratified flow. Part 3. Semi-elliptical obstacle. *J. Fluid Mech. 35*, 481–486.

Lee, J. T., Lawson, R. E., Jr. and Marsh, G. L. 1987. Flow visualization experiments on stably stratified flow over ridges and valleys. *Meterol. Atmos. Phys. 37*, 183–194.

Lilly, D. K. 1978. A severe downslope windstorm and aircraft turbulence induced by a mountain wave. *J. Atmos. Sci. 35*, 59–77.

Lilly, D. K. and Zipser, E. J. 1972. The front range windstorm of 11 January 1972—a meteorological narrative. *Weatherwise 25*, 56–63.

Long, R. R. 1953. A laboratory model resembling the "Bishop wave" phenomenon. *Bull. Amer. Meteor. Soc. 34*, 205–211.

Long, R. R. 1954. Some aspects of the flow of stratified fluids. II. Experiments with a two-fluid system. *Tellus 6*, 97–115.

Long, R. R. 1955. Some aspects of the flow of stratified fluids. III. Continuous density gradients. *Tellus 7*, 341–357.

Miles, J. W. 1969. Waves and wave drag in stratified flows. In: *Proc. 12th Int. Congress Applied Mechanics* (eds. M. Hetenyi and W. G. Vincenti). Berlin: Springer-Verlag, 52–76.

Miles, J. W. and Huppert, H. E. 1979. Lee waves in a stratified flow. Part 4: Perturbation approximations. *J. Fluid Mech. 35*, 497–525.

Peltier, W. R. and Clark, T. L. 1979. The evolution and stability of finite-amplitude mountain waves. Part 2: Surface wave drag and severe downslope windstorms. *J. Atmos. Sci. 36*, 1498–1529.

Peltier, W. R. and Clark, T. L. 1983. Nonlinear mountain waves in two and three spatial dimensions. *Q. J. Roy. Met. Soc. 109*, 527–548.

Rottman, J. W. and Smith, R. B. 1987. Tow-tank simulations of the severe downslope wind. *Proc. Third Int. Symp. Strat. Flows*. Cal. Tech., Pasadena, Calif., 3–5 Feb. 1987.

Smith, R. B. 1985. On severe downslope winds. *J. Atmos. Sci. 42*, 2597–2603.

Smith, R. B. 1987. Aerial observations of the Yugoslavian Bora. *J. Atmos. Sci. 44*, 269–297.

Smith, R. B. and Sun, J.-L. 1987. Generalized hydraulic solutions pertaining to severe downslope winds. *J. Atmos. Sci. 44*, 2934–2939.

Snyder, W. H., Thompson, R. S., Eskridge, R. E., Lawson, R. E., Castro, I. P., Lee, J. T., Hunt, J. C. R. and Ogawa, Y. 1985. The structure of strongly stratified flow over hills: dividing-streamline concept. *J. Fluid Mech. 152*, 249-288.

Thompson R. S. and Snyder, W. H. 1976. EPA fluid modeling facility. *Proc. Conf. on Envir. Modeling and Simulation*, Cincinnati, Ohio. *USEPA Rep. EPA-600/9-76-016*, Washington, D.C.